Journal of Medical Diagnostic Methods
ISSN: 2168-9784

Wang, J Med Diagn Meth 2012, 1:2
DOI: 10.4172/2168-9784.1000106

Research Article

Open Access

SENSE Performance of RF Coil Array at Ultra-High Fields

Shumin Wang*

Department of Electrical and Computer Engineering, Auburn University, Auburn, Alabama, USA

Abstract

The geometrical noise amplification factor (g-factor) of an eight-channel receive-only coil array was studied for brain imaging at various field strengths. At 1.5, 3.0 and 7.0 Tesla, both experimental and simulation results were obtained and compared for verification purposes. Numerical simulations were further performed at 11.7, 14.0 and 21.0 Tesla. It was found that the most significant parallel imaging performance gain was achieved at an acceleration rate 4 and when the field strength is above 3.0 Tesla. However, the performance of parallel imaging plateaus above 11.7 Tesla plateaus due to highly correlated coil profiles.

Keywords: RF coil array; Parallel imaging; High field MRI

Introduction

With the advances of parallel imaging, such as SMASH [1] or SENSE [2], arrays of radio-frequency (RF) coils are now commonly used for MRI signal reception [1,2]. RF coil arrays designed for parallel imaging consist of multiple decoupled coils. Each element is sensitive to a specific region of the entire field of view (FOV) [3]. Combined with a separate volume transmitter, parallel imaging arrays provide the capability of accelerated image acquisition with substantial increases in signal-to-noise ratio (SNR). This feature has been found very beneficial to applications such as BOLD functional MRI [4]. Since the design of receiver array ultimately determines the achievable SNR and parallel imaging performance, many research efforts have been dedicated to SENSE coil design. In [3], a six-element array was optimized for cardiac imaging. In [4], the impacts of some fundamental coil array parameters were examined based on Bio-Savart simulations. It was demonstrated that large number of coils and tightly fitted design generally benefits SENSE imaging. On the contrary, coil overlap should be avoided in general. Because sensitivity profiles are utilized in SENSE for spatial encoding, more distinguished profiles are beneficial to spatial encoding.

A concurrent and prominent development in MRI is high-field systems, i.e., scanner at 7 Tesla and higher field strengths. Such systems deliver the promise of linear SNR increase according to the law of physics. Because RF wavelength is a determinant factor of coil profile, SENSE performance also changes with field strength even if the coil layout remains the same. It is imperative to study this effect in order to guide the design and construction of high-field receiver arrays. In [5] and [6], theoretical studies of the ultimately achievable SNR by parallel imaging were performed by means of plane wave and spherical harmonic basis functions respectively. Both reported that higher field strengths primarily benefit SENSE imaging with high acceleration rates. However, overly-simplified human and RF coil models limit the practicality of these studies. In reality, the anatomy of the human head is much more complicated than a homogeneous water sphere and many design considerations, such as coil overlapping and gapping, can significantly affect the actual SENSE performance [4]. Theoretical studies with hypothetical RF coils cannot take actual design concerns into account and therefore are lack of instructional values. Furthermore, no experimental results were provided to support those theoretical findings and the question is left open as whether they can ever be observed in experiments.

In order to bridge the gap between theory and practice, we performed a detailed study of the SENSE performance of an eight-channel array with respect to field strength. The eight-channel array employed a gapped design which was shown to yield improved SENSE performance [4]. The finite-difference time-domain (FDTD) method was applied to simulate the electromagnetic field distribution inside a human head model, which takes realistic anatomy and coil geometry into account, [7,8]. The numerical simulation was first verified by experimentally measured g-factors of the coil array at 1.5, 3.0 and 7.0 Tesla. The same array was then simulated at 11.7, 14.0 and 21.0 Tesla respectively. It was found that the most significant parallel imaging performance gain was achieved at an acceleration rate 4 and when the field strength is above 3.0 Tesla. However, the performance of parallel imaging plateaus above 11.7 Tesla due to highly correlated coil profiles. Since the highest field strength available for human imaging is 12 Tesla, the results of this study are useful to RF coil design and fabrication for most high-field MRI systems.

Materials and Methods

Eight-Channel head coil arrays

Three eight-channel head coil arrays were built for 1.5, 3.0 and 7.0 Tesla MRI systems respectively. Their geometries are similar, but slightly vary in terms of housing size and element width. The 7.0 Tesla head coil array was designed to fit the average human head (model NMSC25-8-7T, Nova Medical, Wilmington, MA) [9]. It consists of an anterior section and a posterior section separated by a 2 cm intersection gap. Each section has four coil elements mounted on a 2 mm thick fiber glass former. The shape of the anterior former is one quarter of an ellipsoid, whose half axial lengths are 9, 9 and 10 cm respectively. The slightly longer axis is along the anterior-posterior direction. The posterior former consists of two parts. The upper part is the same as the anterior section and the lower part is one half of a 5 cm long elliptical cylinder, whose half axial lengths are 9 and 10 cm. Figure 1a shows a picture of this coil array.

***Corresponding author:** Shumin Wang, Ph.D, Department of Electrical and Computer Engineering, 200 Broun Hall, Auburn University, Auburn, AL 36849-5201, USA, E-mail: SZW0033@auburn.edu

Received August 01, 2012; **Accepted** August 21, 2012; **Published** August 24, 2012

Citation: Wang S (2012) SENSE Performance of RF Coil Array at Ultra-High Fields. J Med Diagn Meth 1:106. doi:10.4172/2168-9784.1000106

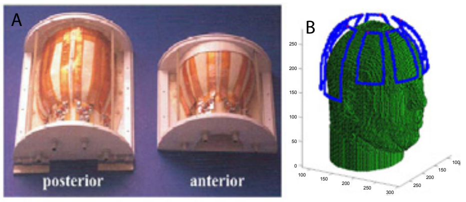

Figure 1: The eight-channel coil array (a) and the computer model (b).

Each coil element was constructed with 1 cm wide copper strips. The shapes of the four coil elements in the same section are identical. In the anterior section, each coil element is trapezoidal when the former is flattened. When measured from center to center, the trapezoid has upper edge length of 2.5 cm, lower edge length of 4.5 cm and side length of 11.5 cm. The inter-coil gap size is 3.5 cm uniformly, which represents 56% coil coverage of the surface area of the former. In the posterior section, each coil element has two parts. The upper part is also trapezoidal. The lower part is a 4.5 cm by 3.5 cm rectangle if the former is flattened. The upper and lower parts form one single coil loop. Gaps between adjacent coil elements are 3.5 cm uniformly. All coils are connected to high-impedance preamplifiers as a means of magnetic decoupling [4].

Experimental results were acquired on 1.5 Tesla Siemens Magnetom, 3.0 Tesla GE Signa LX platforms and 7.0 Tesla GE whole-body scanner respectively. The 1.5 Tesla experiment was similar to that described in [4]. The 7.0 Tesla MRI data were performed by using a 28 cm inner diameter TEM transmit coil, model NM008-7T-GE (Nova Medical, Wilmington, MA). A normal male volunteer was scanned under an IRB-approved protocol (protocol number 03-N-0142). A gradient echo experiment was performed using a 20 ms echo time, 500 ms repetition time, 40° excitation flip angle, 512×384 acquisition matrix, 240×180 mm^2 FOV and 1 mm slice thickness, resulting in a nominal voxel size of 0.5×0.5×1.0 mm^3. Nine oblique-axial slices were acquired in a total acquisition time of 193 s. Phase-sensitive (complex) coil images were reconstructed off-line in IDL (Research Systems, Inc, Boulder, CO, USA). Data were subsequently trimmed to 384×336 voxels (180×156 mm^2 FOV) so that the remaining image narrowly encompassed the head. These trimmed data were used to compute SENSE g-factor maps for both rate-2 and rate-3 acceleration as was described earlier [4].

SNR and g-Factor in SENSE imaging

The relative SNR pertinent to electromagnetic field is defined by [4]

$$SNR \propto \frac{\omega^2 |\vec{B}_1|}{\sqrt{N_s^2 + N_c^2}} \qquad (1)$$

where ω is the angular Lamor frequency, $\vec{B}_1$ is the circularly polarized transverse magnetic field generated by receive coil in transmit mode [10], N_s represents the sample noise and N_c the coil noise. Note that the above defines the relative SNR intrinsic to receive coils, which is not affected by the inhomogeneous transmit coil profiles in high fields. The circularly polarized transverse magnetic field $\vec{B}_1$ is defined by [10].

$$\vec{B}_1 = \frac{\vec{B}_x - i\vec{B}_y}{2} \qquad (2)$$

where $\vec{B}_x$ and $\vec{B}_y$ are the x and y components of the peak complex magnetic flux density.

Sample loss (N_s) mainly originates from thermal effects in the human body [11]. By reciprocity [10], it can be estimated as Ohm loss by

$$N_s \propto \sqrt{\iiint_V \frac{1}{2}\sigma |\vec{E}|^2 \, dv} \qquad (3)$$

Where $\vec{E}$ is the peak complex electric field intensity and σ the tissue conductivity, which is a function of both spatial location and frequency. Coil noise comes from both coil conductors and preamplifiers. At the field strengths being investigated, coil noise is negligible due to their relatively large sizes [4]. Therefore, (1) is reduced to

$$SNR \propto \frac{\omega^2 |\vec{B}_x - i\vec{B}_y|}{\sqrt{\iiint_V \sigma |\vec{E}|^2 \, dv}} \qquad (4)$$

When multiple coil elements are combined in full Fourier encoding, the phase-sensitive combined SNR is [4]

$$SNR_c = \sqrt{\vec{S}^H [\Psi]^{-1} \vec{S}} \qquad (5)$$

where $\vec{S}$ is a vector containing signals contributed from each coil element and $[\Psi]$ is the noise correlation matrix. For well decoupled coil elements, $[\Psi]$ is evaluated by

$$[\Psi]_{i,j} = \iiint_V \frac{1}{2}\sigma \vec{E}_i^* \cdot \vec{E}_j dv \qquad (6)$$

where subscripts indicate contributions from individual coil element. In SENSE imaging, the geometrical amplification factor (g-factor) indicates the penalty incurred by SENSE reconstruction. The SNR now becomes [1]

$$SNR_\rho = \frac{SNR_c}{g_\rho \sqrt{R}} \qquad (7)$$

where both ρ and R denote the acceleration rate. The geometrical noise amplification factor g_ρ is given by [1]

$$g_\rho = \sqrt{\left[\left(\vec{S}^H [\Psi]^{-1} \vec{S}\right)^{-1}\right]_{\rho,\rho} \cdot \left(\vec{S}^H [\Psi]^{-1} \vec{S}\right)_{\rho,\rho}} \qquad (8)$$

FDTD simulation

A 3-by-2.7-by-3 mm model was constructed based on the Brooks' human model for FDTD simulations [12]. The head model consists of 12 different tissues, whose electrical properties at each frequency are obtained by a fourth-order Cole-Cole model [13]. All coil structures were modeled as Perfect Electric Conductors (PEC). On the top of each coil element, one PEC cell was replaced by four transparent current sources as excitation. The actual geometrical modeling of the coil array is shown in figure 1. In this figure, blue color represents PEC cells, green color represents the surface of the human head and red color indicates the signal output. The same geometric setup was applied at all field strengths, thus numerical simulations were able to reveal small changes of SENSE performance that are not easily observable in experiments.

An in-house FDTD program was developed in C++. The FDTD program was compiled on a 2 GHz AMD Opteron 246 processor and run in Linux. Eight layers of Perfectly-Matched-Layer (PML) boundary condition were used in each direction [7]. The entire computational domain consists of 162-by-177-by-147 cells (including the PMLs). The memory requirement was 339 MB. Due to the conditional stability of FDTD [7], the time-step sizes need to be set differently according to the Courant-Fridrich-Levy (CFL) condition at different Larmor frequencies. As the result, the actual CPU time for simulating each coil ranges from 25 minutes (at 21.0 Tesla) to six hours (at 1.5 Tesla).

Results

Figure 2 compares the measured and simulated results at rate-2

Citation: Wang S (2012) SENSE Performance of RF Coil Array at Ultra-High Fields. J Med Diagn Meth 1:106. doi:10.4172/2168-9784.1000106

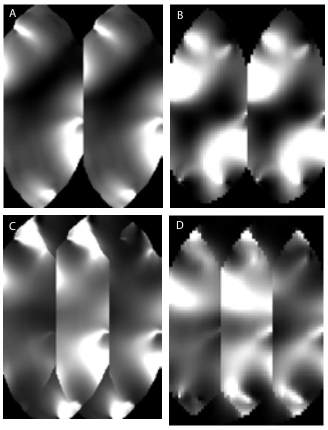

Figure 2: The measured rate-2 (a) and rate-3 (c) g-factor maps and simulated rate-2 (b) and rate-3 (d) g-factor maps at 7.0 Tesla. The scaling factor in all rate-2 maps is 1.2 and that in all rate-3 maps is 1.6. For simulation, the mean value is 1.10 at rate-2 and 1.46 at rate-3. For experiment, the mean value is 1.06 at rate-2 and 1.44 at rate-3.

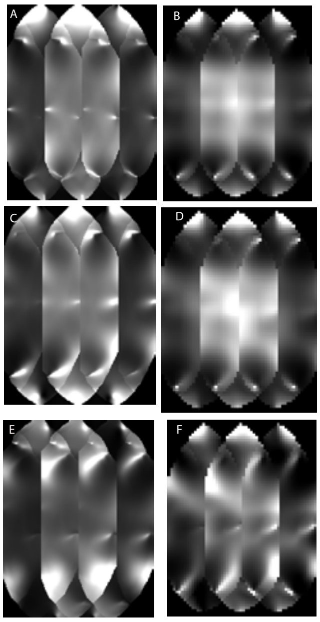

Figure 3: For rate-4 SENSE imaging, the measured g-factor maps at 1.5 Tesla (b), 3.0 Tesla (d) and 7.0 Tesla (f) and the simulated ones at 1.5 Tesla (b), 3.0 Tesla (d) and 7.0 Tesla (f). The scaling factor in all maps is 6.0. For measurements, the mean value is 3.03 at 1.5 Tesla, 2.85 at 3.0 Tesla and 2.69 at 7.0 Tesla. For simulations, the mean value is 2.81 at 1.5 Tesla, 3.09 at 3.0 Tesla and 2.28 at 7.0 Tesla.

and rate-3 at 7.0 Tesla. At both acceleration rates, the simulated and the measured results match well. In figure 3, g-factors at rate-4 are compared at 1.5, 3.0 and 7.0 Tesla respectively. Again, simulation results matched very well with measured data. Next, we extended simulations to 11.7, 14.0 and 21.0 Tesla. To ensure fair comparison, we have maintained the same FOV when calculating all g-Factors. The average g-factor values at different field strengths and different acceleration rates are summarized in figure 4 together with experimental results. It was observed that at all rates, simulated g-factors increase slightly at 3.0 Tesla and then decrease steadily at higher field strengths. The improvement of SENSE performances is also proportional to the acceleration rate. The rate-2 g-factors roughly remain the same. The most significant improvement was observed at rate-4. It was also noticed that g-factor changes are more noticeably below 11.7 Tesla.

Discussion

The simulation and measured SENSE performances were in good agreement in general. However, some discrepancies can be observed in figure 4, which were mainly contributed by the following factors. First of all, coils were modeled by stair-casing in which cubic cells were patched to approximate curved surfaces. This approximation is a main error resource that affects the accuracy of the FDTD. Secondly and perhaps more importantly, the RF coil arrays built for 1.5 and 3.0 Tesla experiments were not exactly the same as the 7.0 Tesla array modeled in simulations. At the same time, the experimental conditions of different scanners cannot be controlled to be exactly the same. It is likely that this difference dictates the observed discrepancies between simulation and experiment data.

The g-factor performances at different field strengths (Figure 4) are related to the field-dependent coil sensitivity profiles. They can be interpreted as the balance between two counter effects. At higher field strengths, the Lamor frequency is higher and the wavelength is shorter. Thus the electrical size (in terms of wavelength) of a coil becomes larger. This is similar to increasing the geometric size of a coil at a fixed field strength. Since larger coils penetrate deeper, which can be seen in figure 5a-5c, their sensitivity profiles are more correlated. Therefore, the noise correlation increases and so does the g-factor. As the field strength further increases to 14.0 Tesla, the so-called dielectric resonance starts to take effect and bright regions appear near the center of the head. This is more pronounced at 21.0 Tesla as shown in figures 5e. The dielectric resonance also makes surface coil sensitivity profiles less independent and further compromises the noise correlation. Since these effects are mainly related to the electrical sizes of coil elements, we denote it as the electrical-size effect. On the other hand, an optimal

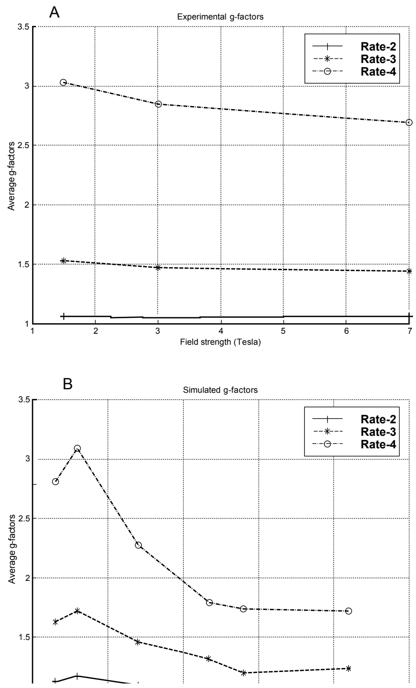

Figure 4: The average measured (a) and simulated (b) g-factors at different field strengths and different acceleration rates.

Citation: Wang S (2012) SENSE Performance of RF Coil Array at Ultra-High Fields. J Med Diagn Meth 1:106. doi:10.4172/2168-9784.1000106

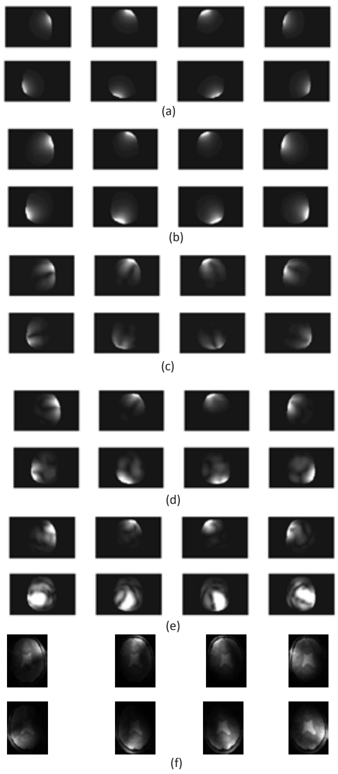

Figure 5: Simulated individual coil profiles at 1.5 Tesla (a), 3.0 Tesla (b), 11.7 Tesla (c), 14.0 Tesla (d) and 21.0 Tesla (e), and measured coil profile at 7.0 Tesla (f). The top row corresponds to the anterior section and the bottom row corresponds to the posterior section.

sensitivity map should have unity signal at the point of interest and zeros at aliasing locations according to the theory of SENSE imaging [5,6]. As the electromagnetic wavelength becomes shorter at higher frequencies, aliasing points are closer and rapid field variations can produce nulls occurring more frequently in space. As the result, SENSE performance tends to improve and the g-factor is expected to decrease at higher field strengths and higher acceleration rates. We denote this as the optimization effect.

The actual performance of a SENSE coil array is the balance between the electrical-size effect and the optimization effect. When the field strength increases from 1.5 Tesla to 3.0 Tesla, the electrical-size effect prevails and the SENSE performance slightly deteriorates (note that this change is so small that it may not be observed due to the uncertainties in experimental conditions). As we further increase the field strength to 11.7 Tesla, the optimization effect is dominant and we observe improved SENSE performances. Above 11.7 Tesla, the electrical-size effect and the optimization effect nearly balance and no significant improvements can be observed.

The SENSE performance can be improved at higher field strengths once the above factors are understood. Because the electrical-size effect is responsible to SENSE performance deteriorations, reducing the geometric sizes of each RF coil would be beneficial. This implies that higher channel-count receiver arrays are preferable in high-field MRI. Nevertheless, the achievable SENSE acceleration rate is ultimately determined by the available SNR that is a function of both field strength and coil design. A densely populated receiver array may not yield high SNR if coil noise becomes dominant [4]. How to balance these factors to achieve optimal SENSE performance will be our future research topic.

Conclusion

The SENSE performance of an eight-channel receive-only head coil array was studied at various field strengths. After verifying numerical simulations with experimental results at 1.5, 3.0 and 7.0 Tesla, simulations were performed at 11.7, 14.0 and 21.0 Tesla. It was found that both the electrical-size effect and the optimization effect contribute to the actual SENSE performance. High-field MRI mainly benefits SENSE imaging when the field strength is beyond 3.0 Tesla with an acceleration rate of no less than 4. These results provide practical guidelines for designing SENSE coil arrays for high-field and high-rate parallel imaging applications.

Acknowledgement

The author thanks Dr. Jacco A. de Zwart for technical assistance.

References

1. Sodickson DK, Manning WJ (1997) Simultaneous acquisition of spatial harmonics (SMASH): fast imaging with radiofrequency coil arrays. Magn Reson Med 38: 591–603.
2. Pruessmann KP, Weiger M, Scheidegger MB, Boesiger P (1999) SENSE: sensitivity encoding for fast MRI. Magn Reson Med 42: 952-962.
3. Weiger M, Pruessmann KP, Leussler C, Roschmann P, Boesiger P (2001) Specific coil design for SENSE: a six-element cardiac array. Magn Reson Med 45: 495-504.
4. de Zwart JA, Ledden PJ, Kellman P, van Gelderen P, Duyn JH (2002) Design of a SENSE-optimized high-sensitivity MRI receive coil for brain imaging. Magn Reson Med 47: 1218-1227.
5. Ohliger MA, Grant AK, Sodickson DK (2003) Ultimate intrinsic signal-to-noise ratio for parallel MRI: electromagnetic field considerations. Magn Reson Med 50: 1018–1030.
6. Wiesinger F, Boesiger P, Pruessmann KP (2004) Electrodynamics and ultimate SNR in parallel MR imaging. Magn Reson Med 52: 376-390.
7. Taflove A (1998) Advances in Computational Electrodynamics: The Finite Difference Time-Domain Method, Artech House, Boston.
8. Collins CM, Smith MB (2001) Signal-to-noise ratio and absorbed power as functions of main magnetic field strength, and definition of "90 degreess" RF pulse for the head in the birdcage coil. Magn Reson Med 45: 684-691.
9. Ledden P, Duyn JH (2002) Ultra-high frequency array performance: predicted effects of dielectric resonance. Proc 10th Annual Meeting ISMRM, Honolulu 324.
10. Insko EK, Elliott MA, Schotland JC, Leigh JS (1998) Generalized Reciprocity. J Magn Reson 131: 111-117.
11. Hoult DI, Bhakar B (1997) NMR Signal Reception: Virtual Photons and Coherent Spontaneous Emission. Concept Magn Reson Part A 9: 277-297.
12. http:/www.brooks.af.mil/AFRL/HED/hedr/hedr.html
13. Gabriel C (1996) Compilation of the Dielectric Properties of Body Tissues at RF and Microwave Frequencies.